© 2016 IJSRSET | Volume 2 | Issue 3 | Print ISSN : 2395-1990 | Online ISSN : 2394-4099
Themed Section: Engineering and Technology

PWM Current-Source Inverter Fed Induction Motor Drive with a New Stator Current Control Method

Kaluri Ramanaiah, Dr. M. BalaSubbareddy
Electrical Engineering Department, Prakasam Engineering College, Kandukur, India

ABSTRACT

In this paper, the control of the pulse width-modulated current-source-inverter-fed induction motor drive is discussed. The vector control system of the induction motor is realized in a rotor-flux-oriented reference frame, where only the measured angular rotor speed and the dc-link current are needed for motor control. A new damping method for stator current oscillations is introduced. The method operates in an open-loop manner and is very suitable for microcontroller implementation, since the calculation power demand is low. Also, the stator current phase error caused by the load filter is compensated without measurement of any electrical variable. With the proposed control methods the motor current sensors can be totally eliminated since the stator current measurements are not needed either for protection in the current-source-inverter-fed drives. The proposed control methods are realized using a single-chip Motorola MC68HC916Y1 micro-controller. The experimental tests show excellent performance in both steady-state and transient conditions.

Keywords: Current-Source Converter, Digital Control, Induc-Tion Motor Drives, Microcontrollers, Vector Control.

I. INTRODUCTION

THE rapid development of power and microelectronics in recent years allows the use of the induction machine also in high-performance motor drives. At low- and medium-power levels the variable-speed induction motor drives are usually re-alized using pulsewidth-modulated (PWM) voltage-source in-verters (PWM-VSIs). However, the switched voltages yield high voltage slopes over the stator windings, which stresses the insulations and causes bearing current problems. A possible solution for this problem is the use of a PWM current-source in-verter (PWM-CSI) (Fig. 1). Both the voltages and the currents of the machine are almost sinusoidal and, therefore, the voltage stresses in the machine windings are lower.

In the PWM-CSIs a C filter has to be inserted on the load side to reduce the current harmonics. Due to the capacitive currents of the filter, the motor current references are not realized accu-rately, which may cause unsatisfactory performance and insta-bility problems. A few methods [1], [2], which are based on the measurement of the stator voltages and/or currents, have been reported to solve the problem. However, the aim in the present paper is to compensate the filter currents without measurements using the steady-state model of the motor and the filter.

On the other hand, the C filter and the machine inductances form a resonance circuit which is stimulated especially when the stator current references are changed. Some methods [3], [4], also based on the measurement of the stator voltages and/or currents, have been proposed to damp the stator current oscilla-tions in the transient conditions. However, in PWM-CSI drives, stator current measurements are not needed for protection since the overcurrent can be detected with the dc-link current sensor. It is, therefore, preferable to use control methods where stator current measurements are not needed, because in that case the motor current sensors can be totally eliminated.

In the present paper, the control system of the PWM-CSI-fed induction motor is under investigation. The line-side converter has been studied earlier [5] when the prototypes of 5 and 100 kW were also built. The proposed vector control system is realized in the rotor-

flux-oriented reference frame. The capac-itive currents of the load filter are compensated without stator current or voltage measurements. A new method for damping the stator current oscillations in the transient conditions is presented. The method is based on the combined dynamic equations of the load filter and the motor and does not need any electrical feedback variables. Furthermore, the method is suitable for the single-chip microcontroller implementation because the calculation power demand is reasonably low. The proposed control system is realized using a single-chip Motorola MC68HC916Y1 microcontroller.

II. METHODS AND MATERIAL

1. Vector Control of The PWM-CSI-FED Induction Motor Drive

Fig. 1 shows the main circuit of the PWM-CSI-fed induction motor drive. L_{lif} and C_{lif} are the inductance and capacitance of the line filter and u_{sup} the supply voltage. C_{lof} is the load filter capacitance. The line and load bridges are identical. Both bridges consist of six controllable switches such as insulated gate bipolar transistors (IGBTs). Antiparallel diodes of the IGBTs in the commercial power modules are also shown in the figure. Because of these diodes and the very low reverse voltage-blocking capability of traditional IGBTs, additional diodes have to be connected in series with the transistors. However, the new IGBTs with reverse blocking capability are being launched on the markets, which makes the series diodes unnecessary [6]. L_{dc} is a smoothing inductor which is often split in two and connected in both bars of the dc circuit to minimize the bearing current problems of the motor drive [7].

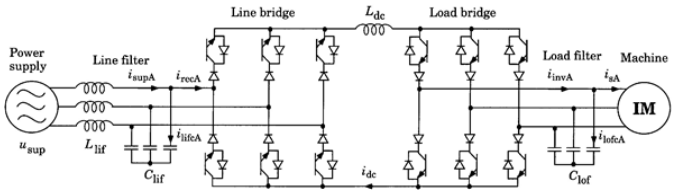

Figure 1. Main circuit of the PWM-CSI-fed induction motor drive.

In the PWM-CSI drives the line converter is used to control the dc-link current. The function of the line converter is synchro-nized with the supply voltages. By changing a modulation index in the line bridge, the dc-link voltage, i.e., the dc-link current, can be controlled. On the other hand, if the phase-shift angle between the modulation references and the supply voltages is varied from zero, the reactive power level can be adjusted to the desired level. The line filter takes reactive power which can be compensated by the control system.

The stator currents are generated by the load converter. The load filter takes capacitive currents which are proportional to the square of stator frequency in the constant-flux region and linearly proportional to the stator frequency in the field-weak-ening region.

A. Rotor-Flux-Based Motor Control System

In the vector control strategies, the ac motors are controlled like dc motors which have independent channels for flux and torque control. The electromagnetic torque of the induction motor in the rotor-flux-oriented reference frame can be written as [8]

$$t_e = \frac{3}{2} p \frac{L_m^2}{L_r} |\boldsymbol{i}_{mr}| i_{sy} \qquad (1)$$

where p is the number of pole pairs, L_m magnetizing induc-tance, L_r rotor self-inductance, $|\boldsymbol{i}_{mr}|$ rotor magnetizing cur-rent, and i_s the imaginary axis component of the stator current vector in the rotor-flux-based coordinate system. Below nom-inal rotor speed, $|\boldsymbol{i}_{mr}|$ is kept constant and the electromagnetic torque is controlled with i_s. Above nominal rotor speed, the reference value of the magnetizing current is reduced to keep the stator voltage at an acceptable level. In the rotor-flux-ori-ented reference frame $|\boldsymbol{i}_{mr}|$ can be controlled with the real axis component of the stator current vector i_{sx} as follows [8]:

$$i_{sx} = T_r \frac{d}{dt} |\boldsymbol{i}_{mr}| + |\boldsymbol{i}_{mr}| \qquad (2)$$

where T_r is rotor time constant.

Fig. 2(a) shows the block diagram of both line and load con-verter control systems. The vector control system of the induc-tion motor is realized in the rotor-flux-oriented reference frame and is based on an indirect vector control scheme [8]. The y component of the stator current reference vector i_s is obtained as the output signal of the speed controller. The x component of the stator current reference vector i_s is generated according to magnetizing current reference using (2). These two

vectors form the inverter current reference vector $\boldsymbol{i}_{mr*}$ expressed in the rotor-flux-oriented reference frame. It is transformed to the sta-tionary reference frame as follows:

$$\boldsymbol{i}^*_{\mathrm{inv}} = \boldsymbol{i}^{mr*}_{\mathrm{inv}} e^{j\theta_{mr}}. \quad (3)$$

The magnetizing current reference value is generated by FG1.

$|\boldsymbol{i}_{mr*}|$ is kept constant below nominal rotor speed, and above nominal speed the magnetizing current reference value is in-versely proportional to the rotor speed. In the indirect vector control system the rotor flux angle θ_{mr} is calculated as a sum of the measured rotor angle and the ref-erence value of the slip angle in the following way [8]:

$$\theta_{mr} = \theta_r + \theta^*_{\mathrm{sl}} = \theta_r + \int \omega^*_{\mathrm{sl}}\, dt = \theta_r + \int \frac{i^*_{sy}}{T_r |\boldsymbol{i}^*_{mr}|} dt. \quad (4)$$

If the angular rotor speed ω_r instead of θ_r is measured, as is the case in Fig. 2(a), (4) can be written as

$$\theta_{mr} = \int \omega_{mr}\, dt = \int (\omega_r + \omega^*_{\mathrm{sl}})\, dt = \int \left(\omega_r + \frac{i^*_{sy}}{T_r |\boldsymbol{i}^*_{mr}|}\right) dt. \quad (5)$$

After coordinate transformation the inverter current reference vector is fed to the modulator. The current-source PWM con-verter has six active and three zero switching vectors [9]

$$\boldsymbol{i}_n = \frac{2}{\sqrt{3}} i_{\mathrm{dc}} e^{j(2n-1)\pi/6}, \qquad \text{for } n = 1, 2, \ldots 6 \quad (6)$$

and

$$\boldsymbol{i}_n = 0, \qquad \text{for } n = 7, 8, 9. \quad (7)$$

The reference vector is realized using the two limiting active vectors of the sector as shown in Fig. 3.

The modulation times of the active switching vectors within the modulation period T_m can be calculated as follows:

$$T_n = \left|\frac{\boldsymbol{i}^*_{\mathrm{inv}}}{i_{\mathrm{dc}}}\right| \sin\left(\frac{\pi}{3} - \gamma\right) T_m = m \sin\left(\frac{\pi}{3} - \gamma\right) T_m \quad (8)$$

$$T_{n+1} = \left|\frac{\boldsymbol{i}^*_{\mathrm{inv}}}{i_{\mathrm{dc}}}\right| \sin(\gamma) T_m = m \sin(\gamma) T_m \quad (9)$$

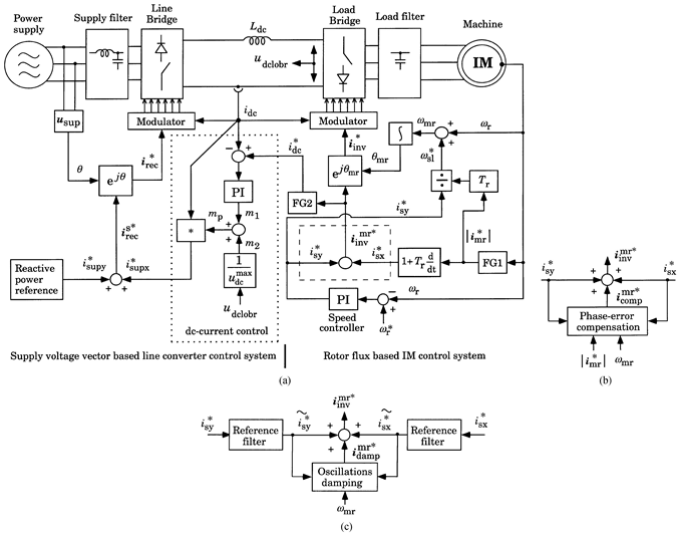

Figure 2. (a) Control system of the PWM-CSI-fed induction motor drive. (b) Compensation of the stator current phase error. (c) Damping of the stator current oscillations.

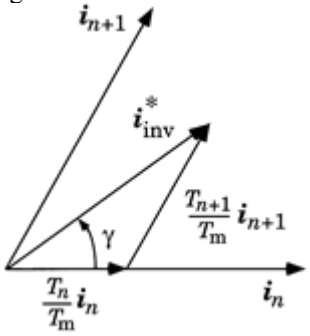

Figure 3. Realization of the inverter current reference vector with two switching expressed in terms of the quadrature components of the supply vectors.

where the constant , i.e., the magnitude of the dc-link current should be equal or greater than the length of the inverter current reference vector in order to keep the modulation in the linear region.

B. Supply-Voltage-Vector-Based Line Converter Control System

The control system of the line converter is realized in the syn-chronously rotating reference frame where the real axis is tied to the supply voltage vector. In the supply-voltage-based reference frame, the active and reactive power of the line converter can be voltages and currents with the following two simple equations:

$$T_o = T_m - T_n - T_{n+1}. \quad (10)$$

The dc-link current reference value is generated in Fig. 2(a) by FG2 as follows:

$$i_{\mathrm{dc}}^{*} = c\,|\boldsymbol{i}_{\mathrm{inv}}^{mr*}| = c\sqrt{(i_{\mathrm{inv}x}^{*})^2 + (i_{\mathrm{inv}y}^{*})^2} \qquad (11)$$

$$p = \frac{3}{2} u_{\mathrm{sup}x} i_{\mathrm{sup}x} \qquad (12)$$

and

$$q = -\frac{3}{2} u_{\mathrm{sup}x} i_{\mathrm{sup}y}. \qquad (13)$$

The block diagram of the line converter control system is shown in Fig. 2(a). The component of the supply current reference vector i^{*}_{supx} is obtained as the output signal of the dc-link cur-rent control. The component of the supply current reference vector i^{*}_{supy} is generated according to reactive power reference using (13).

In the dc current control the total modulation index corresponding to active power is constructed as the sum of the modulation index obtained as an output of the propor-tional–integral (PI) controller and the modulation index obtained from the feedforward control. In the feedforward control is generated by dividing the measured dc voltage

of the load bridge u_{dclobr} by the maximum dc voltage of the line bridge $u_{\mathrm{dc}}^{\max} = 3/\sqrt{2}U_{\mathrm{sup}}$ where U_{sup} is the rms value of the phase supply voltage. By using feedforward control the dynamics and the stability of the dc current control can be Improved. Finally, the component of the supply current reference vector $i_{\mathrm{sup}x}^{*}$ is constructed as a product of the measured dc-link current i_{dc} and active power modulation index. m_p

It is also possible to compensate the reactive power drawn by the line filter and to damp the supply current oscillations without any measurements. However, these control methods are not in-cluded in the block diagram shown in Fig. 2(a). The complete description of the line converter control can be found in [5]

C. Compensation of the Stator Current Phase Error

The problem in the Fig. 2(a) control system is that the stator current references are not realized accurately because of the ca-pacitive currents drawn by the load filter. The combined steady-state equations of the load filter and motor, expressed in the rotor-flux-oriented reference frame, can be used to compensate the stator current error caused by the load filter. Next, the equa-tions needed for compensation control are derived.

The stator voltage equation of the induction motor in the sta-tionary reference frame can be expressed as [8]

$$\boldsymbol{u}_s = R_s \boldsymbol{i}_s + \sigma L_s \frac{d\boldsymbol{i}_s}{dt} + (1-\sigma) L_s \frac{d\boldsymbol{i}_{mr}}{dt} \qquad (14)$$

where $\sigma = 1 - L_2/(L_s L_r)$ is the resultant leakage constant. The load filter capacitor voltage can be written as

$$\boldsymbol{u}_{\mathrm{lofc}} = \frac{1}{C_{\mathrm{lof}}} \int \boldsymbol{i}_{\mathrm{lofc}}\, dt \qquad (15)$$

and the load capacitor current

$$\boldsymbol{i}_{\mathrm{lofc}} = \boldsymbol{i}_{\mathrm{inv}} - \boldsymbol{i}_s. \qquad (16)$$

By substituting (16) into (15) and the resulting equation into (14) ($\boldsymbol{u}_s = \boldsymbol{u}_{\mathrm{lofc}}$) the following expression is obtained:

$$\frac{1}{C_{\mathrm{lof}}} \int (\boldsymbol{i}_{\mathrm{inv}} - \boldsymbol{i}_s)\, dt = R_s \boldsymbol{i}_s + \sigma L_s \frac{d\boldsymbol{i}_s}{dt} + (1-\sigma) L_s \frac{d\boldsymbol{i}_{mr}}{dt}. \qquad (17)$$

$$+ (1-\sigma) L_s C_{\mathrm{lof}} \frac{d}{dt}|\boldsymbol{i}_{mr}| + j2\omega_{mr} \frac{d}{dt}|\boldsymbol{i}_{mr}| - \omega_{mr}^2 |\boldsymbol{i}_{mr}| \Big] + \boldsymbol{i}_s^{mr} \qquad (18)$$

where $\omega_{mr} = d\theta_{mr}/dt$. According to (18) the effect of load filter in the steady state can be compensated as follows:

$$\boldsymbol{i}_{\mathrm{comp}}^{mr} = jR_s C_{\mathrm{lof}} \omega_{mr} \boldsymbol{i}_s^{mr} - \sigma L_s C_{\mathrm{lof}} \omega_{mr}^2 \boldsymbol{i}_s^{mr} - (1-\sigma) L_s C_{\mathrm{lof}} \omega_{mr}^2 |\boldsymbol{i}_{mr}|. \qquad (19)$$

The stator resistance term in (19) is neglibly small and can be ignored. When the resulting equation is expressed in terms of direct- and quadrature-axes components we have

$$i_{\mathrm{comp}x}^{*} \approx -\sigma L_s C_{\mathrm{lof}} \omega_{mr}^2 i_{sx}^{*} - (1-\sigma) L_s C_{\mathrm{lof}} \omega_{mr}^2 |\boldsymbol{i}_{mr}^{*}| \qquad (20)$$

and

$$i_{\mathrm{comp}y}^{*} \approx -\sigma L_s C_{\mathrm{lof}} \omega_{mr}^2 i_{sy}^{*} \qquad (21)$$

where the reference values of the stator current components and the rotor magnetizing current are used. In the constant-flux re-
gion $i_{sx} = |\boldsymbol{i}_s|$ and (20) can be written as

$$i_{\mathrm{comp}x}^{*} \approx -L_s C_{\mathrm{lof}} \omega_{mr}^2 i_{sx}^{*}. \qquad (22)$$

The proposed compensation method is shown in the block dia-gram form in Fig. 2(b), which replaces the area surrounded by the broken line in Fig. 2(a).

D. Damping of the Stator Current Oscillations

The load filter capacitance and the machine inductances form a resonance circuit which is stimulated especially

when the stator current references are changed. One solution to overcome this problem is to use combined dynamic equations of the load filter and the motor. With the dynamic equations the stator currents can be controlled in such a way that the impulses for oscillations are eliminated.

By taking into consideration the dynamic terms of the stator current vector in (18) we have

$$\boldsymbol{i}_{\mathrm{damp}}^{mr} = R_s C_{\mathrm{lof}} \frac{d\boldsymbol{i}_s^{mr}}{dt} + \sigma L_s C_{\mathrm{lof}} \frac{d^2\boldsymbol{i}_s^{mr}}{dt} + j2\sigma L_s C_{\mathrm{lof}} \omega_{mr} \frac{d\boldsymbol{i}_s^{mr}}{dt}. \tag{23}$$

The dynamic terms of rotor magnetizing current are not in-cluded in (23) because $|\boldsymbol{i}_{mr}|$ changes much more slowly than $\boldsymbol{i}_{mr}$ and also because the rotor magnetizing current is normally kept constant. When (23) is expressed in terms of direct- and quadrature-axes components we have

When (17) is solved for the inverter current $\boldsymbol{i}_{\mathrm{inv}}$ and expressed $-2\sigma LC\omega \frac{di_{sy}}{dt}$ (24) in the rotor-flux-based reference frame we have

$$\boldsymbol{i}_{\mathrm{inv}}^{mr} = R_s C_{\mathrm{lof}} \left[\frac{d\boldsymbol{i}_s^{mr}}{dt} + j\omega_{mr} \boldsymbol{i}_s^{mr} \right] + \sigma L_s C_{\mathrm{lof}} \left[\frac{d^2\boldsymbol{i}_s^{mr}}{dt} + j2\omega_{mr} \frac{d\boldsymbol{i}_s^{mr}}{dt} - \omega_{mr}^2 \boldsymbol{i}_s^{mr} \right]$$

$$i_{\mathrm{dampx}}^{*} = R_s C_{\mathrm{lof}} \frac{d\tilde{i}_{sx}^{*}}{dt} + \sigma L_s C_{\mathrm{lof}} \frac{d^2\tilde{i}_{sx}^{*}}{dt}$$

and

$$i_{\mathrm{dampy}}^{*} = R_s C_{\mathrm{lof}} \frac{d\tilde{i}_{sy}^{*}}{dt} + \sigma L_s C_{\mathrm{lof}} \frac{d^2\tilde{i}_{sy}^{*}}{dt} + 2\sigma L_s C_{\mathrm{lof}} \omega_{mr} \frac{d\tilde{i}_{sx}^{*}}{dt}.$$

However, because, in practice, real stator currents cannot follow the step responses of the stator current references, modified (filtered) current references (i_{s*} and i_{s*}) are used in (24) and (25). The proposed current damping method is shown in Fig. 2(c), which again replaces the area surrounded by the broken line in Fig. 2(a). The stator current phase-error compensation and the oscillations damping methods can be combined when the block diagrams of Fig. 2(b) and (c) are connected in parallel.

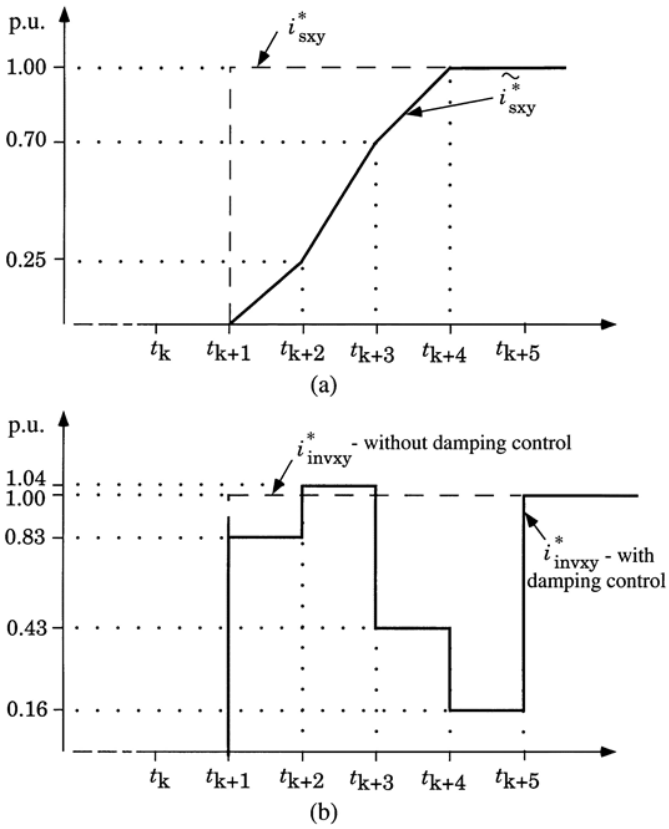

An example of filtering the stator current references is shown in Fig. 4(a) where the subscript refers to both stator current vector components. The unit step change of the stator current reference vector component is plotted with the broken line and the filtered stator current reference with the solid line. A change in stator current reference value is obtained at time. The realization of the reference value is begun at time because of the onetime interval calculation delay. The filtering is com-pleted after three time intervals.

For microcontroller implementations (24) and (25) must be discretized when we have

$$i_{\mathrm{dampx}}^{*,k+1} = R_s C_{\mathrm{lof}} \left(\frac{\Delta\tilde{i}_{sx}^{*}}{\Delta t} \right)^{k+1} + \sigma L_s C_{\mathrm{lof}} \left[\frac{\Delta \left(\frac{\Delta\tilde{i}_{sx}^{*}}{\Delta t} \right)}{\Delta t} \right]^{k+1} - 2\sigma L_s C_{\mathrm{lof}} \omega_{mr} \left(\frac{\Delta\tilde{i}_{sy}^{*}}{\Delta t} \right)^{k+1} \tag{26}$$

Table I. Test Parameters

Motor:	
Nominal stator phase voltage U_{sN}	220 V
Nominal stator current I_{sN}	6.2 A
Nominal shaft power P_N	2.2 kW
Number of pole pairs p	3
Nominal speed n_N	940 r/min
Magnetizing inductance L_m	155 mH
Stator leakage inductance L_{sl}	7.2 mH
Rotor leakage inductance L_{rl}	7.2 mH
Stator resistance R_s	2.3 Ω
Rotor resistance R_r	1.8 Ω
Converter:	
Load filter capacitance C_{lof}	8 µF
Dc-link inductance L_{dc}	30 mH
Line filter capacitance C_{lif}	8 µF
Line filter inductance L_{lif}	2.3 mH

$$i_{\mathrm{damp}y}^{*,k+1} = R_s C_{\mathrm{lof}} \left(\frac{\Delta \tilde{i}_{sy}^{*}}{\Delta t} \right)^{k+1} + \sigma L_s C_{\mathrm{lof}} \left[\frac{\Delta \left(\frac{\Delta \tilde{i}_{sy}^{*}}{\Delta t} \right)}{\Delta t} \right]^{k+1} + 2\sigma L_s C_{\mathrm{lof}} \omega_{mr} \left(\frac{\Delta \tilde{i}_{sx}^{*}}{\Delta t} \right)^{k+1} \quad (27)$$

where (both components combined in one expression)

$$\left(\frac{\Delta \tilde{i}_{sxy}^{*}}{\Delta t} \right)^{k+1} = \left(\tilde{i}_{sxy}^{*,k+2} - \tilde{i}_{sxy}^{*,k+1} \right) / \Delta t \quad (28)$$

and

$$\left[\frac{\Delta \left(\frac{\Delta \tilde{i}_{sxy}^{*}}{\Delta t} \right)}{\Delta t} \right]^{k+1} = \left[\left(\frac{\Delta \tilde{i}_{sxy}^{*}}{\Delta t} \right)^{k+1} - \left(\frac{\Delta \tilde{i}_{sxy}^{*}}{\Delta t} \right)^{k} \right] \Big/ \Delta t. \quad (29)$$

In discrete realization the average values of modified stator cur-rent references during a time interval should be used in the sum-ming point shown in Fig. 2(c). These can be expressed as

$$\tilde{i}_{sxy,\mathrm{av}}^{*,\,k+1} = \left(\tilde{i}_{sxy}^{*,\,k+2} - \tilde{i}_{sxy}^{*,\,k+1} \right) / 2. \quad (30)$$

Finally, the modified stator current reference, which is filtered according to Fig. 4(a), can be written as

$$\tilde{i}_{sxy}^{*,k+2} = \tilde{i}_{sxy}^{*,k+1} + 0.25 \left(i_{sxy}^{*,k+1} - i_{sxy}^{*,k} \right) + 0.45 \left(i_{sxy}^{*,k} - i_{sxy}^{*,k-1} \right) + 0.3 \left(i_{sxy}^{*,k-1} - \tilde{i}_{sxy}^{*,k-2} \right). \quad (31)$$

With typical load filter and motor parameters, like those given in Table I, the effect of the first and third terms on the right side of (26) and (27) in damping control are neglibly small and the following approximation can be made:

$$i_{\mathrm{damp}xy}^{*,k+1} \approx \sigma L_s C_{\mathrm{lof}} \left[\frac{\Delta \left(\frac{\Delta \tilde{i}_{sxy}^{*}}{\Delta t} \right)}{\Delta t} \right]^{k+1}. \quad (32)$$

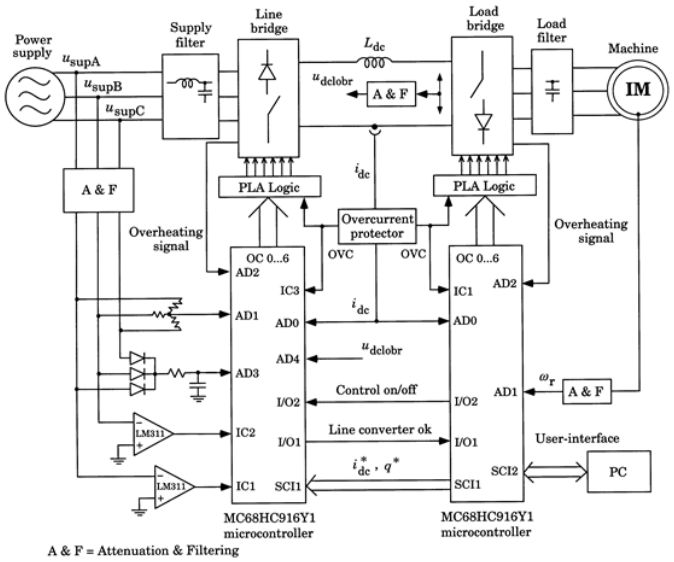

Figure 5. Microcontroller implementation of the PWM-CSI-fed induction motor drive.

Fig. 4(b) shows the inverter current reference components with (—) and without (– –) the damping method resulting from the Fig. 4(a) unit step change. Without damping control if the motor current phase-error compensation method is not used as is done in Fig. 4(b) to simplify the description of the damping algorithm. With damping control is calculated using (30) and (32) and the parameters shown in Table I. The discrete time interval is 200 s.

The dynamics of the stator current can be controlled with the selection of coefficients in (31). In vector-controlled motor drives it is important that current references are realized quickly in order to achieve dc-motor-like dynamic performance. Oth-erwise, if the step responses of the stator current reference components are realized very quickly, high inverter current pulses are needed according to (26)–(29) which increases the magnitude of the dc current and in that way the power losses of the converter. For that reason, the selection of the refer-ence filter algorithm is a compromise between the dynamics and efficiency of the motor drive. In the case of Fig. 4 the coefficients of the reference algorithm are selected so that the highest inverter current pulses needed have approximately the same magnitude as the original current reference (1 p.u.). This way the dc current is not increased to an excessively high level but good performance is still achieved.

In practice, the motor parameters are not constant but change due to the magnetic saturation and the temperature variation. As a result, the motor inductances needed in the proposed con-trol methods should be known at various operating points to guarantee fine load filter current compensation and current os-cillation damping. The effect of the temperature variation on the rotor time constant, which is needed in rotor flux angle calcu-lation, can be compensated, e.g., with the thermal model of the machine [8].

III. RESULTS AND DISCUSSION

Experimental Investigation

The vector-controlled PWM-CSI-fed induction motor drive is realized using the parameters shown in Table I. Both bridge circuits are built using 1200-V 50-A IGBTs. The line and load filter capacitors are wye connected.

The control system realization of both converters is based on the Motorola MC68HC916Y1 16-bit single-chip micro-controller whose main features are: 48-kB on-chip FLASH EEPROM, 4-kB on-chip RAM, 8- or 10-bit A/D-converter with eight input channels, general-purpose timer (GPT), time processing unit (TPU), 2* serial communication interfaces (SCIs), 0.5-μs 16×16 fractional multiply, and 1.5-μs 32/16 divide (at 16-MHz clock frequency).

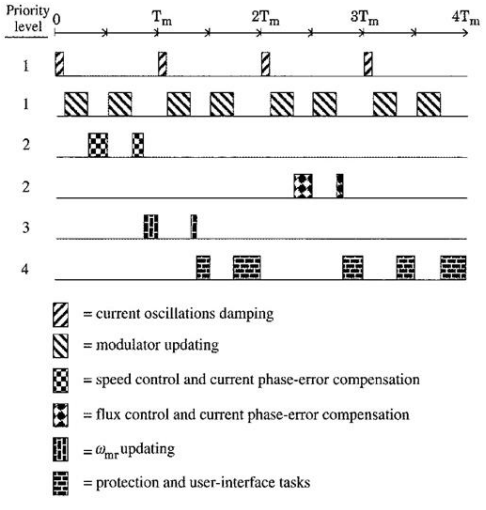

Figure 6. Time scheduling between the motor control software procedures

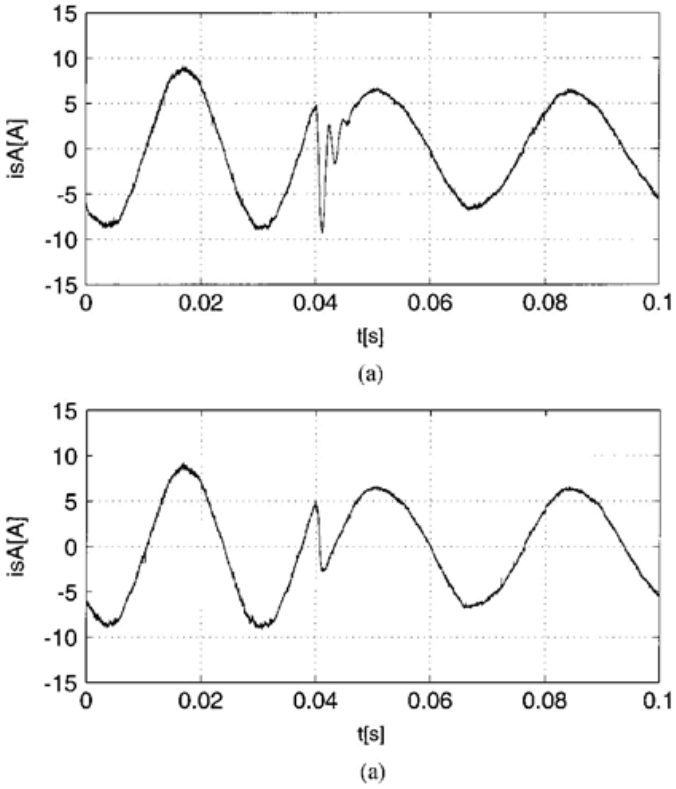

Figure 7. Experimental waveforms of phase-A stator current at sudden change in i . (a) Without oscillation damping control. (b) With damping control.

The block diagram of the microcontroller implementation is shown in Fig. 5. The function of the drive is headed by the control system of the load converter. The dc-link current and the reactive power reference values are transmitted to the line converter control system via serial connection (SCI1). The user interface is realized with a personal computer (PC) which is connected to the second SCI (SCI2) of the load converter microcontroller.

The modulation signals of both bridges are generated using seven output compare (OC) signals (OC0...OC6) of the TPU and external programmable logic array (PLA) circuit [10]. The angular rotor speed is measured with an analog tachometer whose signal, after attenuation and filtering, is connected to the input of the A/D converter (AD1) in the load converter control system. The measured dc current (AD0) and the dc voltage of the load bridge (AD4) are needed in the line converter for dc current control. The measured dc current (AD0) is needed in the load converter only for modulator realization. The overcurrent protection is realized with an external protector, which dis-ables the modulation signals generated by the PLA logic. This

overcurrent signal (OVC) is also connected to input capture channels in line (IC3) and load converter (IC1) control systems, which are polled by the software. The complete description of the line converter microcontroller implementation can be found in [5].

The software procedures and the time scheduling between the motor control tasks are shown in Fig. 6. The time scheduling is based on the interrupts made by the timer unit. The interrupts are generated twice in every modulation period. The modula-tion frequency is set to 5 kHz, resulting in an interrupt rate of 100 μs. The software procedures are divided into four different priority levels. At the highest level are the stator current oscilla-tions damping and the modulator updating. The damping control is executed every second interrupt time and it is realized using (30) and (32). The modulation times are calculated every inter-rupt time with (8)–(10) where $T_m/2$ instead of T_m is used. The sine function between $0...\pi/3$ needed in (8) and (9) is calcu-lated in advance and stored in on-chip FLASH memory. How-ever, before modulation time calculation the rotor flux angle is computed by integrating the angular rotor flux speed according to (5). In discrete form this can be given as

$$\theta_{mr}^{k+1} = \theta_{mr}^{k} + \omega_{mr} T_m/2. \qquad (33)$$

At the second level are the speed and flux control, which are done every eighth interrupt time after high-priority-level tasks. In the speed control a conventional PI algorithm is used. In the flux control the x -axis component of the stator current reference vector is calculated according to (2), which can be written in discrete form as

$$i_{sx}^{*,k+1} = T_r \frac{\left|\boldsymbol{i}_{mr}^{*,k+1}\right| - \left|\boldsymbol{i}_{mr}^{*,k}\right|}{\Delta t} + \left|\boldsymbol{i}_{mr}^{*,k+1}\right|. \qquad (34)$$

After speed and flux control tasks the stator current phase error is compensated using (20)–(22). If the second level tasks are not finished before the next time-scheduling interrupt they are continued after high-priority tasks in the next period. At the third level is the angular rotor flux speed updating and it is begun every 16th interrupt time. The expression for ω_{mr} can be found in (5). At the lowest priority level are the protection and the user interface tasks and these are done at the main program level.

Fig. 7 shows the test results of the current oscillations damping method. The y component of stator current reference vector is suddenly changed at time instant 40 ms. Fig. 7(a) and (b) show the results without and with damping control, respectively. The test results show that oscillations can be significantly reduced with the proposed damping method.

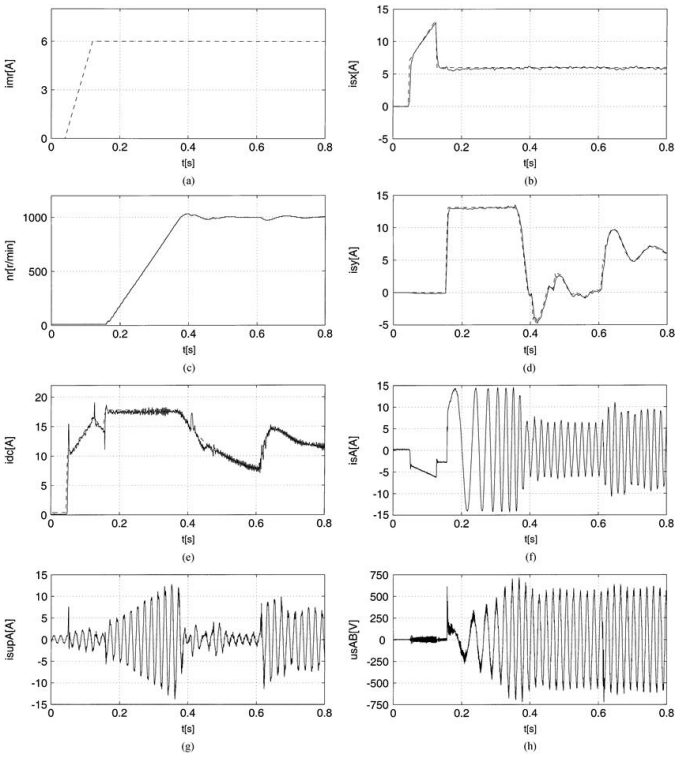

Figure 8. Experimental results of the vector-controlled induction motor drive. (a) Magnetizing current reference jij. (b) x-axis stator currenti. (c) Rotor speed n. (d)y-axis stator current i. (e) DC currenti. (f) Phase-A stator currenti. (g) Phase-A supply current i. (h) Stator main voltage u.

Fig. 8 shows the experimental results of the whole vector-controlled motor drive. The reference values are plotted with the broken line and the measured values with the solid line. The control system of the inverter includes the proposed methods to compensate the stator current phase error and to damp the stator current oscillations. Also, the control system of the line rectifier includes the compensation of the reactive power drawn by the supply filter and the damping of the supply current oscillations.

The magnetization of the motor is begun at 50 ms. The reference value of the rotor magnetizing current is rate limited in order to keep i_s at an acceptable level. It should be noted that the transient in the phase-A supply current in Fig. 8(g) at 50 ms is not caused by the resonance of the *LC* filter but by the characteristics of the dc current controller. Due to the overshoot in dc

current the energy is first stored in and then restored from the dc circuit until the dc current reaches its reference value, which causes the spikes in the supply current. Then, at about 150 ms the reference value of the rotor speed is changed from 0 to 1000 r/min and finally at about 600 ms the load torque is changed from 0 to nominal value (22 N m). The dc current reference value is calculated using in (11). Negative slopes of are filtered using time constant of 100 ms. The output of the speed controller is limited to. The results show that the operation of the drive is stable. Also, it can be concluded that the measured stator currents follow the stator current references closely and that the oscillations in the stator currents are low.

IV. CONCLUSION

In this paper the control of the PWM-CSI-fed induction motor in the rotor-flux-based reference frame has been discussed. New methods for compensating the error between the reference and measured value of the stator current caused by the load filter and for damping the stator current oscillations, when the stator current references are changed, without feedback variables have been presented. The proposed control methods enable the elimi-nation of the stator current sensors since the stator current mea-surements are not needed either for protection. The tests with the prototype show that with the proposed control methods the stability of the drive can be considerably improved.

V. REFERENCES

[1] J. Cambronne, B. Semail, and C. Rombaut, "Vector control of a P.W.M. current source inverter-fed induction motor," in Proc. 4th Eur. Conf.Power Electronics and Applications, vol. 2, Florence, Italy, 1991, pp.177–181.

[2] A. Dakir, R. Barlik, M. Novak, and P. Grochal, "Computer simulations for two angular-speed-control systems of a current source inverter feeding an induction machine," in Proc. IEEE Int. Symp. IndustrialElectronics, vol. 2, 1996, pp. 940–945.

[3] D.-C. Lee, D.-H. Kim, and D.-W. Chung, "Control of PWM current source converter and inverter system for high performance induction motor drives," in Proc. 22nd Int. Conf. Industrial Electronics, Controland Instrumentation, vol. 2, 1996, pp. 1100–1105.

[4] P. Eichenberger and M. Junger, "Predictive vector control of the stator voltages for an induction machine drive with current source inverter," in Proc. 28th Annu. IEEE Power Electronics Specialists Conf., vol. 2, 1997, pp. 1295–1301.

[5] M. Salo and H. Tuusa, "A vector controlled current-source PWM rec-tifier with a novel current damping method," IEEE Trans. Power. Elec-tron., vol. 15, no. 3, pp. 464–471, May 2000.

[6] A. Lindemann, "Characteristics and applications of a reverse blocking IGBT," in Proc. PCIM Europe, Jan.–Feb. 2001, pp. 12–16.

[7] T. Halkosaari and H. Tuusa, "Reduction of conducted emissions and motor bearing currents in current source PWM inverter drives," in Proc.30th Annu. IEEE Power Electronics Specialists Conf., vol. 2, 1999, pp.959–964.

[8] P. Vas, Electrical Machines and Drives. London, U.K.: Oxford Univ. Press, 1992.

[9] B. H. Kwon and B. Min, "A fully software-controlled PWM rectifier with current link," IEEE Trans. Ind. Electron., vol. 40, no. 3, pp. 355–363, Jun. 1993.

[10] M. Salo and H. Tuusa, "A microcontroller implementation of a vector controlled current-source PWM-rectifier," in Proc. Nordic WorkshopPower and Industrial Electronics, Espoo, Finland, 1998, pp. 31–36.